Acoustic Resonance Frequencies of Underwater Toroidal Bubbles

M Alloul, B Dollet, O Stephan, E Bossy, C Quilliet, P Marmottant

Acoustic Resonance Frequencies of Underwater Toroidal Bubbles

M. Alloul, B. Dollet, O. Stephan, E. Bossy, C. Quilliet, and P. Marmottant*
Univ. Grenoble Alpes, CNRS, LIPhy, F-38000 Grenoble, France

(Received 11 March 2022; revised 10 June 2022; accepted 12 September 2022; published 23 September 2022)

Underwater bubbles display an acoustic resonance frequency close to spherical ones. In order to obtain a resonance significantly deviating from the spherical case, we stabilize bubbles in toroidal frames, resulting in bubbles which can be slender while still compact. For thin tori the resonance frequency increases greatly. Between a pair of bubble rings, we can achieve a flat acoustic pressure field for a critical distance between rings, a condition reminiscent of Helmholtz coils in magnetostatics. This opens the possibility to shape the acoustic field using long tunnels of rings.

DOI: 10.1103/PhysRevLett.129.134501

Introduction.—Underwater bubbles are very good resonators when excited by acoustic waves. Spherical bubbles were the most studied, featuring a resonance frequency known as the Minnaert frequency [1]. Deviations from the spherical shape were investigated with ellipsoidal bubbles [2] showing a small deviation in frequency, less than 10% for an aspect ratio of 4, but hardly with other shapes.

Our motivation is to understand if bubbles can highly depart in resonance frequency from the spherical case. The originality of the present study is to investigate toroidal bubbles that feature two characteristic lengths: a small one (the small radius b of the torus) and a large one (the grand radius R of the torus). Cylinders have the same property, but tori are more compact.

Toroidal bubbles are found in nature and in applications. Such bubbles are on purpose emitted by dolphins during their aquatic evolutions [3] as part of play. They are encountered in cavitation studies, where they constitute the ultimate stage of collapsing bubbles close to rigid boundaries [4]. Entrapped within a vortex ring, these bubbles are always in motion [5,6], which makes them difficult to study.

Recently, we demonstrated that we can trap and stabilize bubbles within open frames. Not only are such stabilized bubbles very good building blocks to build new acoustic metamaterials with novel acoustic properties [7–13], but they open the way to study arbitrary shapes. For frames assuming the shape of regular Platonic solids, the resonance frequency was found to be close to spherical bubbles with the same volume within a few percent [14,15].

This Letter describes the capture of stable toroidal bubbles and the measurement of their acoustic properties as a function of their shape. Toroidal shapes are a good candidate to show original resonance properties, owing to their specific topology and the possibility to tune the aspect ratio R/b between the grand radius R and the small radius b; see Fig. 1(a).

Design, fabrication, and immersion.—Toroidal open frames were designed from a mainly hexagonal mesh, with hexagonal openings as monodisperse as possible (in order to avoid a large opening that would be a point of entry for water). The method was to build a triangular mesh using SURFACE EVOLVER [16], and then to consider its dual, which is obtained by taking the centers of the triangles and linking neighbor centers [see Fig. 1(b) and further details in Supplemental Material [17]]. We obtain a computer model of the frames by placing spheres at the centers and bars for

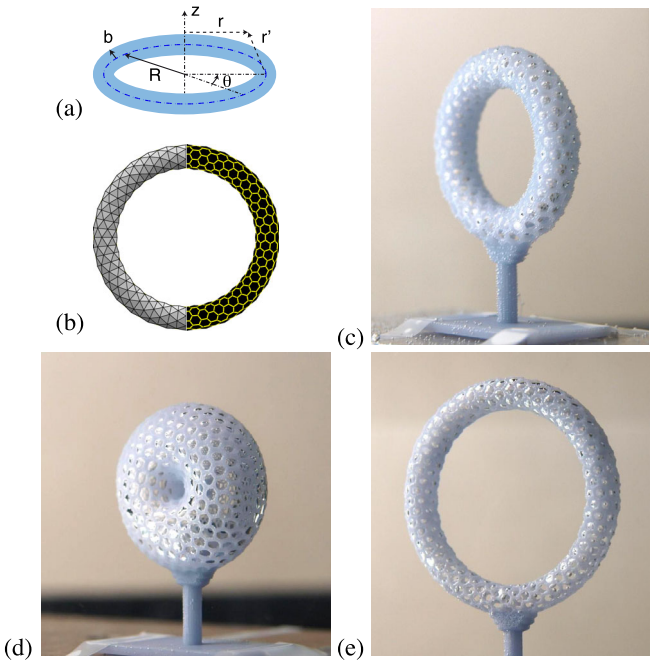

FIG. 1. (a) Torus dimensions and coordinates. (b) Design of the toroidal frames: triangular mesh (left) and dual mesh (right). (c)–(e) Bubble entrapped after immersion of frames with several aspect ratios: (c) $R/b = 4.5$, (d) 1.31, (e) 7.4. The grand radii of these structures are (c) $R = 8$, (d) 4.8, and (e) 11.3 mm.

the links (script in FreeCAD). We manufactured frames by 3D stereolithography to obtain millimetric frames, made hydrophobic by silanization. Note that the diameter d of the inscribed circle of the openings is between 66% and 72% of the diameter of the inscribed circle of the almost plane hexagonal faces Then we immersed the toroidal ring with its symmetry axis vertical, in order to reduce the hydrostatic pressure difference between the bottom of the structure and the water level during partial immersion. Capillary pressure holding the interfaces at the bottom of the structure was large enough to resist hydrostatic pressure ($4\sigma/d > \rho g H$, with σ the surface tension and H the height during immersion). After complete immersion their axis can be rotated to be horizontal as in Figs. 1(c)–1(e).

Resonance frequency.—The toroidal bubbles were excited by an underwater speaker as in Refs. [14,15] with frequency sweeps. We recorded the bubble acoustic emission with a hydrophone located around 1 cm away from it. We extracted the relative contribution of the bubble to the signal by computing $A = (\hat{P} - \hat{P}^0)/\hat{P}^0$, where $\hat{P}$ and $\hat{P}^0$ are the Fourier transforms of the hydrophone measurements with and without the bubble. The resonance frequency was measured as the frequency for which the phase of the contribution is shifted by $\pi/2$, corresponding to a peak in the amplitude of the contribution. We measured the resonance frequency for different torus volumes V and aspect ratios R/b. Instead of the gas volume, we used the equivalent radius $R_{\mathrm{eq}} = [V/(4\pi/3)]^{1/3}$ to compare to the vibration of spheres of the same volume. We found that the frequency of toroidal bubbles is always higher than spheres [Fig. 2(a)]. The ratio of the resonance frequency to that of spheres of the same volume is an increasing function of the aspect ratio [Fig. 2(b)]. High-aspect-ratio tori with $R/b = 12$ feature a resonance that is nearly 60% higher, which is a large relative deviation from the Minnaert frequency, as compared to the deviation observed for Platonic shapes investigated so far, of the order of a few percent only [14,15].

Analytical model for a thin torus.—This original behavior can be modeled analytically considering a toroidal gas-liquid interface, neglecting the influence of the structure. Previous results on cubic structures showed no noticeable influence of the frames, provided the inscribed circle diameter of the holes was greater than 60% of the face inscribed diameter [15], which is the case here.

We describe the volume pulsation by considering an oscillation of the small radius with time $b(t)$ for a grand radius R fixed. We consider the limit of a thin torus, $R/b \gg 1$. Any point in space has cylindrical coordinates r, z. We note r' the distance to the grand circle in the middle of the torus [Fig. 1(a)].

Close to the bubble surface, at a distance r' such that $r' \ll R$, the flow field is the one around a pulsating cylinder, with a radial velocity $u = b\dot{b}/r'$ (dots denoting time derivatives). The velocity potential Φ (giving the flow field $\mathbf{u} = \boldsymbol{\nabla}\Phi$) writes in this region $\Phi_{\mathrm{close}} = b\dot{b}\ln(r'/r_0)$, with r_0 a yet unknown variable linked to the system size.

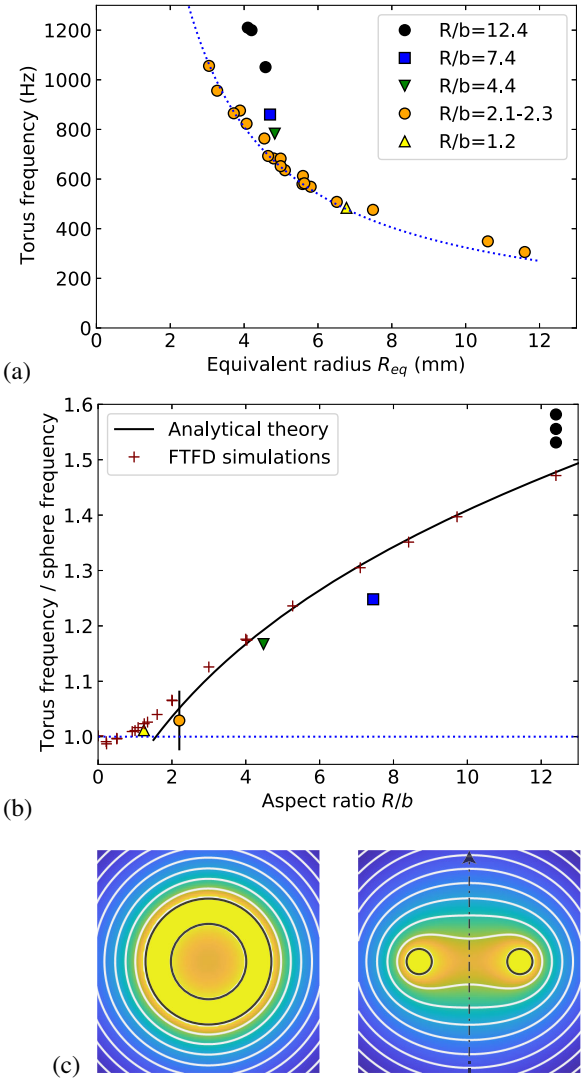

FIG. 2. (a) Resonance frequency of tori as a function of the equivalent radius R_{eq} (the radius of the gas volume packed in a sphere) with different aspect ratio R/b. The blue dotted line shows the frequency of a sphere. (b) Resonance frequency compared to that of sphere of same volume, as a function of aspect ration R/b. Line: analytical model for a thin torus [Eq. (2)]; crosses: 3D finite-difference time-domain (FDTD) simulations; dotted line: frequency of the sphere. (c) Simulations of the emitted field of a torus ($R/b = 4$): cross section $z = 0$ (left) and $\theta = \mathrm{const}$ (right). White lines: isopressure contours, chosen to be equidistant for a field decaying as $1/r$.

Away from the surface, in the region $r' \gg b$, we can assimilate the torus to an infinitely thin circular ring. When the bubble pulsates with a bubble wall velocity $\dot{b}$, each portion of length $Rd\theta$ located at position $\mathbf{r}_c(\theta)$ acts as a source of flow rate $dQ = 2\pi b\dot{b}Rd\theta$, with a velocity potential, evaluated at observation position $\mathbf{r}$, equal to $d\Phi(\mathbf{r}) = -dQ/(4\pi|\mathbf{r} - \mathbf{r}_c|)$. Hence, the velocity potential

of a pulsating ring writes $\Phi_{\text{away}}(\mathbf{r}) = -\frac{1}{2}Rb\dot{b}\int_0^{2\pi} d\theta/|\mathbf{r}-\mathbf{r}_c|$. Evaluating this integral yields $\Phi_{\text{away}} = -(2Rb\dot{b}/\sqrt{(r+R)^2+z^2})K(4Rr/((r+R)^2+z^2))$, with K the complete elliptical integral of the first kind.

We can match the two expressions of the potential in the intermediate region $b \ll r' \ll R$. In this region the outer potential approximates $\Phi_{\text{away}} \simeq b\dot{b}\ln(r'/8R)$, using the known series expansion $K(1-m) = -\frac{1}{2}\ln(1-m) + 2\ln 2 + \mathcal{O}[(1-m)\ln(1-m)]$. This yields $r_0 = 8R$, and solves the value of the potential in the vicinity of the bubble.

Now we consider an applied acoustic pressure $p_a(t)$ in addition to the ambient pressure p_0. At distances large compared to R but small compared to the acoustic wavelength λ, the velocity potential tends to zero, and the pressure tends to $p_0 + p_a(t)$ (note that $\lambda \gg R$ holds, since λ is of order 1 m in the kilohertz range of frequencies encountered in this study). The flow being irrotational and incompressible, Bernoulli's theorem ensures that $\rho(\partial\Phi/\partial t) + \frac{1}{2}\rho\mathbf{u}^2 + p$ is uniform in the liquid. Considering small-amplitude vibrations ($|b-b_0| \ll b_0$), hence neglecting nonlinear terms, and looking in the region near the surface where $\Phi = b\dot{b}\ln(r'/8R)$, we thus obtain the pressure at the bubble surface: $p_{\text{surf}} \simeq p_0 + p_a(t) + \rho b_0\ddot{b}\ln(8R/b_0)$. Now, the continuity of normal stress at the bubble surface yields $p_{\text{surf}} = p_b$, with p_b the inner pressure of the bubble, neglecting surface tension. Assuming an adiabatic behavior of the gas [18], we get $p_b = p_0(b_0/b)^{2\gamma} \simeq p_0[1-2\gamma(b-b_0)/b_0]$, where $\gamma = 1.4$ is the specific heat ratio. We therefore have $\rho b_0\ddot{b}\ln(8R/b_0) + 2\gamma p_0(b-b_0)/b_0 = p_a(t)$, whence the resonance frequency:

$$\omega_t^2 = \frac{2\gamma p_0}{\rho b_0^2 \ln(8R/b_0)}. \tag{1}$$

The effect of the aspect ratio of the torus appears through the logarithmic term $\ln(8R/b_0)$. This relates to other fields of physics governed by Laplace equation, notably the dynamics of vortex rings in hydrodynamics [5,19] or the capacitance of charged rings in electrostatics [20].

We can compare the resonance frequency of the torus and that of the sphere of the same volume V, which verifies $\omega_s^2 = 3\gamma p_0/\rho R_{\text{eq}}^2$, with R_{eq} the sphere radius [21]. Since $V = 2\pi^2 R b_0^2 = 4\pi R_{\text{eq}}^3/3$, we readily obtain

$$\frac{\omega_t^2}{\omega_s^2} = \left(\frac{2\pi^2}{3}\right)^{1/3} \frac{R^{2/3}}{b_0^{2/3}\ln(8R/b_0)}, \tag{2}$$

which is an increasing function of the aspect ratio. Hence, it is possibly to design "high-pitched" bubble of a given volume by using thin tori. This asymptotic prediction compares very well to both experimental data [Fig. 2(b)] and predictions from finite-difference time-domain (FDTD) simulations [Fig. 2(c)], even down to $R/b = 2$; here, simulations were performed with the freeware SimSonic [22], following the approach detailed in Ref. [14]. The scatter in experimental data is likely due to the uncertainty on the exact location of the air-liquid interfaces.

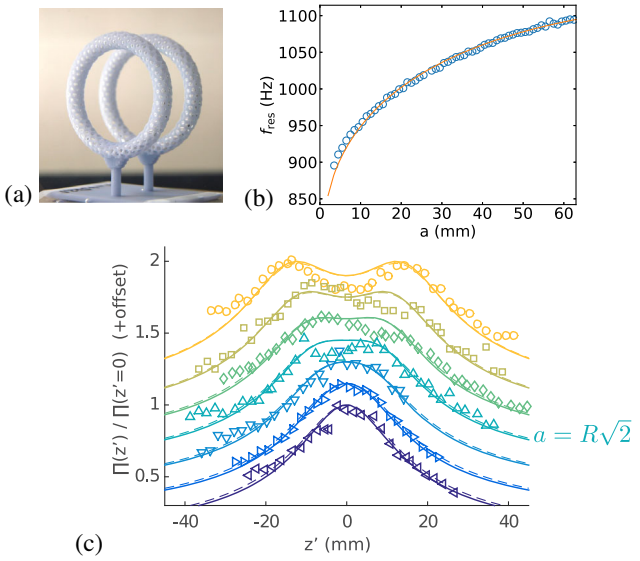

FIG. 3. (a) Two coaxial rings as in Fig. 1(d) with centers separated by a distance $a = 11.25$ mm. (b) Resonance frequency f_{res} versus the distance a between two tori of aspect ratio 11.9 and radii $R = 15.8$ mm. Circles: experimental data. Plain curve: fit by $f_0 = \omega_-/2\pi$, with ω_- given by Eq. (4), where $\omega_t = 1.18$ kHz is obtained as a free fitting parameter. (c) Pressure field versus the coordinate z' along the axis ($z' = 0$ at the mass center of the tori system), for two tori of aspect ratio 7.4 (and $R = 11.35$ mm) separated by distances $a = 3$ (◁), 7 (▷), 12 (▽), 16 (△, fulfilling $a = R\sqrt{2}$), 19 (◇), 23 (□), and 28 mm (○). The experimental pressure field is fitted by $\Pi(z')$ given by Eq. (5) with a multiplicative prefactor as fitting parameter, then rescaled by $\Pi(z'=0)$ (continuous lines). In order to display how the gap changes the dependence in z with optimal clarity, the curves have been shifted by arbitrary offsets, equal to 0, 0.15, 0.3, 0.45, 0.6, 0.75, and 0.9, respectively, for $a = 3$, 7, 12, 16, 19, 23, and 28 mm. 3D simulations (dashed lines) are also featured.

For smaller values of R/b, the analytical prediction based on the thin-torus approximation breaks down as expected. FDTD simulations are, however, valid for any R/b values, including both fat tori ($R/b \gtrsim 1$) and self-intersecting tori ($0 < R/b < 1$). As illustrated in Fig. 2(b), the frequency ratio smoothly tends to 1 when R/b decreases to 0, corresponding to the spherical case.

Two rings.—Having obtained the response of one ring, we explored the interaction of a couple of coaxial rings [Fig. 3(a)]. A first noticeable effect is that the resonance frequency (lowest mode) quickly decreases when the rings are approaching each other [Fig. 3(b)], as is the case for two spheres approaching each other [23].

Remarkably, when recording the pressure generated by the bubble pair along the axis for different pair distances,

we found that at large distance a (between the centers of the rings) the pressure profile has two separate peaks separated by a minimum, and this minimum transforms in a flat plateau for closer distances, before yielding a unique peak [Fig. 3(c)]. Therefore, there is a separation for which the pressure is almost constant in a wide area. This phenomenon is reminiscent of Helmholtz coils used to produce quasiuniform magnetic fields [24].

The two identical coaxial tori constitute a system of coupled oscillators. To predict the eigenfrequencies of this system, we extend the previous theory for thin tori. By linear superposition, the velocity potential equals $\Phi' = -(2Rb_0\dot{b}_1/\sqrt{(r+R)^2+(z'+a/2)^2})K(4Rr/((r+R)^2+(z'+a/2)^2)) - (2Rb_0\dot{b}_2/\sqrt{(r+R)^2+(z'-a/2)^2})K(4Rr/((r+R)^2+(z'-a/2)^2))$, where (r,z') are the cylindrical coordinates with respect to the center of symmetry of the system. Here, torus i ($i=1,2$), of instantaneous radius $b_i(t)$, is centered at $r=0$, $z'=(-1)^i a/2$. Assuming $a \gg b_0$, the evaluation of Φ' at the surface of torus 2 of equation $(r-R)^2+(z'-a/2)^2=b_0^2$ yields $\Phi' \simeq -b_0[\dot{b}_1 f_t(R/a)+\dot{b}_2\ln(8R/b_0)]$, with a coupling factor $f_t(\xi)=(2\xi/\sqrt{4\xi^2+1})K(4\xi^2/4\xi^2+1)$. We then evaluate the pressure at the surface of torus 2, and from the continuity of normal stress, we get

$$\rho b_0\left[\ddot{b}_1 f_t\left(\frac{R}{a}\right)+\ddot{b}_2\ln\frac{8R}{b_0}\right]+2\gamma p_0\frac{b_2-b_0}{b_0}=-p_a(t), \qquad (3)$$

and a similar equation is found by swapping indices 1 and 2. Hence, the eigenfrequencies are the roots of the equation:

$$\begin{vmatrix} \omega^2-\omega_t^2 & \omega^2\frac{f_t(R/a)}{\ln(8R/b_0)} \\ \omega^2\frac{f_t(R/a)}{\ln(8R/b_0)} & \omega^2-\omega_t^2 \end{vmatrix}=0,$$

using the expression of the single-torus eigenfrequency [Eq. (2)], whence

$$\omega_\pm^2=\omega_t^2\left[1\mp\frac{f_t(R/a)}{\ln(8R/b_0)}\right]^{-1}. \qquad (4)$$

The lowest eigenfrequency ω_- corresponds to the two bubbles oscillating in phase, while ω_+ corresponds to the two bubbles oscillating in antiphase. Since the pressure emitted by the bubbles comes mostly from volume oscillations [21], we measure only ω_-. Equation (4) shows that ω_- is lower than the eigenfrequency of a single torus, and is an increasing function of the distance a, since $f_t(\xi)$ is an increasing function of ξ. This prediction is in qualitative agreement with the acoustic interactions of two spherical bubbles [25].

From Bernoulli's theorem, the pressure emitted by the vibrating tori equals $p_t(r=0,z')=-\rho\partial\Phi'/\partial t=\pi\rho b_0\ddot{b}\Pi(z')$, with

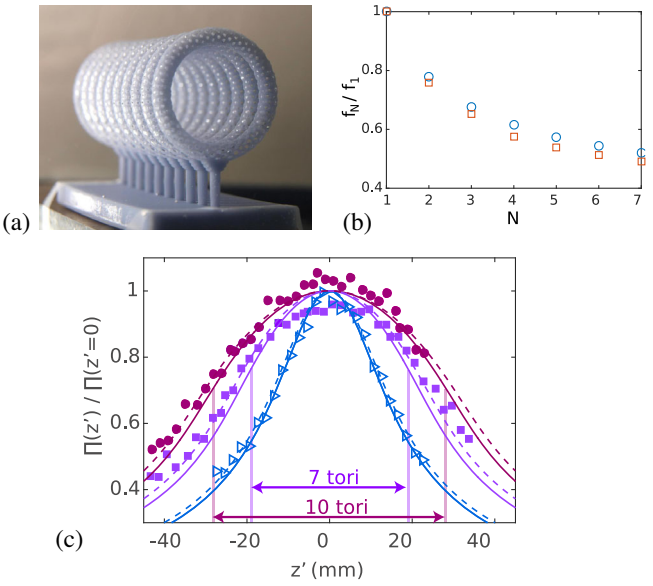

FIG. 4. (a) Tunnel of toroidal bubbles equally spaced by $a=6.25$ mm ($R=11.35$ mm and $R/b=7.4$). (b) Ratio of the resonance frequency for N tori to the single-torus resonance versus the number of tori: experimental data (□) and predictions (○). (c) Pressure field, fitted and rescaled as in Fig. 3(c), versus the coordinate z' along the axis, for two (▷), seven (■), and ten (•) tori with almost the same distance between adjacent tori: $a=7$ mm for the two tori, $a=6.25$ mm for the other cases. Continuous lines: theory. Dashed lines: simulations. Vertical lines indicate the position of the ends of the seven and ten tori tunnels.

$$\Pi(z')=\frac{R}{\sqrt{R^2+(z'-a/2)^2}}+\frac{R}{\sqrt{R^2+(z'+a/2)^2}}, \qquad (5)$$

where Π is the dimensionless function which encompasses the spatial dependence of the pressure field. It decays as $1/z'$ far from the tori, but its behavior between the tori depends on a; it is easy to show that Π presents a single maximum at the middle of the two tori for $a<R\sqrt{2}$, but two symmetric maxima and a local minimum at the middle of the two tori for $a>R\sqrt{2}$. The critical condition $a=R\sqrt{2}$ corresponds to a very flat profile at the middle of the two tori, This critical distance for a "flattest" pressure profile is reminiscent of Helmholtz coils. However, the Helmholtz condition is $a=R$ because of the difference ranges of magnetostatics ($\sim 1/z'^2$) versus pressure ($\sim 1/z'$) fields produced by circular sources. This prediction is in very good agreement with the experiments and 3D simulations [Fig. 3(c)].

Multiple rings.—In order to enhance the extent of the domain with a uniform pressure field we manufactured a series of equally spaced coaxial rings [Fig. 4(a)]. Increasing the number of rings has two effects. First, the collective resonance frequency drops noticeably when the number of rings increases [Fig. 4(b)]. Second, the width (and the magnitude) of the pressure peak increases with the number

of rings, as shown of Fig. 4(c). We obtain a tunnel with a strong pressure, of amplitude around 8 times the excitation pressure.

The previous theoretical analysis can be easily generalized to an arbitrary number N of coaxial tori with a distance a between two consecutive tori: for i between 1 and N, we denote $z = (i - (N + 1/2))a$ the position of torus i along the symmetry axis of the tori. For this torus, accounting for the coupling to all other tori, Eq. (3) can be generalized to $\rho b_0[\sum_{j=1,j\neq i}^{N} \ddot{b}_j f_t(R/a|i-j|) + \ddot{b}_i \ln(8R/b_0)] + 2\gamma p_0(b_i/b_0) = -p_a(t)$. This results in a linear system of N equations for the eigenfrequencies, which must be solved numerically. Like for the two-torus case, the lowest eigenfrequency corresponds to oscillations in phase of all tori, and it is the one which is measured experimentally [see comparison Fig. 4(b)]. The pressure field is a superposition of the ones emitted by each torus, and reproduce the measurements quite well [Fig. 4(c)].

Perspectives.—Toroidal bubbles are convenient elements to shape the acoustic field, and to obtain extended regions of long and uniform pressure, which provides a new tool for acoustic applications such as acoustic trapping of particles [26,27]. They can be packed in numbers, to obtain original acoustic metamaterials. At the ocean level, we hypothesize that dolphins should already be aware of the acoustic properties of rings since they often emit pulsed sounds when making rings. In particular, they should be able to detect a "glissando" toward higher resonance frequencies when a ring enlarges, increasing the aspect ratio R/b at constant gas volume.

*philippe.marmottant@univ-grenoble-alpes.fr

[1] M. Minnaert, Philos. Mag. J. Sci. **16**, 235 (1933).
[2] Z. Ye, J. Acoust. Soc. Am. **101**, 681 (1997).
[3] K. Marten, K. Shariff, S. Psarakos, and D. J. White, Sci. Am. **275**, 82 (1996).
[4] E. A. Brujan, G. S. Keen, A. Vogel, and J. R. Blake, Phys. Fluids **14**, 85 (2002).
[5] T. J. Pedley, J. Fluid Mech. **32**, 97 (1968).
[6] J. K. Walters and J. F. Davidson, J. Fluid Mech. **17**, 321 (1963).
[7] D. R. Smith, J. B. Pendry, and M. C. K. Wiltshire, Science **305**, 788 (2004).
[8] V. Leroy, A. Strybulevych, M. G. Scanlon, and J. H. Page, Eur. Phys. J. E **29**, 123 (2009).
[9] A. Bretagne, A. Tourin, and V. Leroy, Appl. Phys. Lett. **99**, 221906 (2011).
[10] T. Brunet, A. Merlin, B. Mascaro, K. Zimny, J. Leng, O. Poncelet, C. Aristégui, and O. Mondain-Monval, Nat. Mater. **14**, 384 (2015).
[11] V. Leroy, A. Strybulevych, M. Lanoy, F. Lemoult, A. Tourin, and J. H. Page, Phys. Rev. B **91**, 020301(R) (2015).
[12] Z. Cai, S. Zhao, Z. Huang, Z. Li, M. Su, Z. Zhang, Z. Zhao, X. Hu, Y.-S. Wang, and Y. Song, Adv. Funct. Mater. **29**, 1906984 (2019).
[13] T. Combriat, P. Rouby-Poizat, A. A. Doinikov, O. Stephan, and P. Marmottant, Soft Matter **16**, 2829 (2020).
[14] M. Harazi, M. Rupin, O. Stephan, E. Bossy, and P. Marmottant, Phys. Rev. Lett. **123**, 254501 (2019).
[15] M. Boughzala, O. Stephan, E. Bossy, B. Dollet, and P. Marmottant, Phys. Rev. Lett. **126**, 054502 (2021).
[16] K. Brakke, Exp. Math. **1**, 141 (1992).
[17] See Supplemental Material at http://link.aps.org/supplemental/10.1103/PhysRevLett.129.134501 for the design of the cages and an overview of the experimental set-up.
[18] The gas of thermal diffusivity $\chi = 2.2 \times 10^{-5}\,\mathrm{m}^2/\mathrm{s}$, oscillating at angular frequency ω, behaves quasiadiabatically if the thermal penetration depth $\sqrt{\chi/\omega}$ is much smaller than b_0. Anticipating Eq. (1) for the resonance frequency, where we neglect the logarithmic term for simplicity (and with no consequence on the order of magnitude of the current evaluation), we find that the quasiadiabatic limit holds provided $b_0 \gg \chi\sqrt{\rho/p_0} = 2\ \mu\mathrm{m}$, a condition that is amply met in our experiments.
[19] P. G. Saffman, *Vortex Dynamics* (Cambridge University Press, Cambridge, England, 1993).
[20] *Electrodynamics of Continuous Media (Second Edition)*, edited by L. Landau and E. Lifshitz, 2nd ed., Course of Theoretical Physics Vol. 8 (Pergamon, Amsterdam, 1984).
[21] T. G. Leighton, *The Acoustic Bubble* (Academic Press, London, 1994).
[22] www.simsonic.fr.
[23] M. Strasberg, J. Acoust. Soc. Am. **25**, 536 (1953).
[24] J. D. Jackson, *Classical Electrodynamic* (Wiley, New York, 1999), 3rd ed.
[25] E. A. Zabolotskaya, Acoust. Phys. **30**, 365 (1984).
[26] H. Bruus, Lab Chip **12**, 1014 (2012).
[27] D. Baresch and V. Garbin, Proc. Natl. Acad. Sci. U.S.A. **117**, 15490 (2020).